Analysis of key genes and immune infiltration in ruptured intracranial aneurysms based on artificial neural networks and bioinformatics

Qi Jia
Affiliated Hospital of Nantong University
Wei-Hua Shi
The First Affiliated Hospital of Guangxi Medical University
Xiao-Jian Lu
Affiliated Hospital of Nantong University
Shu-Qing Sun
Affiliated Hospital of Nantong University
Jun-Jie Shao
Affiliated Hospital of Nantong University
Qing-Feng Huang (qingfenghuangcf025@ntu.edu.cn)
Affiliated Hospital of Nantong University

Research Article

Keywords: Artificial neural network, bioinformatics, disease signature gene, immune infiltration, intracranial ruptured aneurysm

Posted Date: May 18th, 2022

DOI: https://doi.org/10.21203/rs.3.rs-1644936/v1

Abstract

Background: Intracranial aneurysm (IA) is a potentially devastating cerebrovascular disease, and its rupture leads to subarachnoid hemorrhage with high mortality and disability rates. This study aimed to predict the potential biomarkers of ruptured intracranial aneurysms (RIAs) and explore the correlation between RIAs and immune infiltration through artificial neural networks and bioinformatics analysis.

Method: Three RIA gene microarray data sets were obtained from the gene expression profile (GEO) database, with GSE13353 and GSE36791 as the training sets and GSE54083 as the validation set. Differentially expressed genes (DEGs) were obtained after the analysis. The Kyoto Encyclopedia of Genes and Genomes, Gene Ontology, and Metascape databases were used for functional enrichment analysis. A random forest tree was used to screen for disease signature genes, while a neural network model was built afterward. The accuracy was also confirmed in the validation set. Finally, immune cell infiltration in the unruptured IAsand RIAs groups was analyzed using CIBERSORT.

Results: A total of 27 DEGs were identified by the analysis, 1 of which was a downregulated gene and 26 were upregulated genes. The functional enrichment associated with RIAs was closely related to inflammation and immune function. Hexokinase 3, matrix metalloproteinase 9, CST7, NCF2, and uridine phosphorylase 1 were disease signature genes for RIAs and could be used as potential markers for predicting RIAs. The numbers of CD8+ T cells, CD4+ memory T cells, activated natural killer cells, macrophages M0, and neutrophils were high in the RIA group in immune cell infiltration analysis.

Conclusion: The analysis revealed disease signature genes and immune cell infiltration types that predicted RIAs and had important effects on inflammatory and immune responses.

Introduction

Intracranial aneurysm (IA) is a potentially devastating cerebrovascular disease characterized by the pathological dilatation of the intracerebral arterial wall to form a cystic bulge [1]. Unruptured IAs (UIAs) occur in middle-aged and elderly people in the 40–60 age group, with a prevalence of up to 3.2% [2]. A majority of patients with UIAs often have no obvious clinical manifestations and are diagnosed on examination. However, some patients are still admitted to the hospital as an emergency with IA rupture leading to subarachnoid hemorrhage. Aneurysm rupture occurs in approximately 1% of patients with IA each year [3], resulting in a mortality rate of 30–40% and a disability rate of approximately 50% among survivors [2]. The prognosis is often poor. Therefore, further studies on the molecular mechanisms of its formation, development, and rupture are necessary for public health.

Inflammation and immune response have been recognized as important influences in the development of IA [4]. Immune cell infiltration plays an essential role in the pathogenesis of many diseases, both oncologic and nononcologic, but the study on RIAs needs to be further refined. Artificial neural networks (ANNs) can model nonlinear relationships in high-dimensional data sets and play a key role in the field of predictive modeling. Their powerful performance and significantly improved accuracy have a wide range

of applications in the exploration of new therapeutic targets and new cellular biomarkers [5]. In this study, an ANN predictive model was developed for identifying RIAs based on bioinformatics to screen and analyze the disease signature genes of RIAs. The immune cell infiltration associated with RIAs was also evaluated to provide a reference for studying the mechanism of the occurrence of RIAs.

Materials And Methods

Data collation and collection

Three IA gene expression data sets, GSE13353, GSE36791, and GSE54083, were downloaded from the public GEO database. The "SVA" package in the R software was applied to eliminate the batch effect between the GSE13353 and GSE36791 microarray data and combined as the analysis data set. GSE54083 was used as the validation data set. The UIAs were used as the control group. The RIAs were considered the experimental group.

Differentially expressed gene analysis and enrichment analysis

The analysis data sets were filtered using the "Limma, ggplot2" package in the R software with the thresholds of $P < 0.05$ and $|logFC| > 1$. The differentially expressed genes (DEGs) were filtered, and the results were visualized using the "pheatmap" package to create a volcano and heat maps. The DEGs were enriched for Gene Ontology (GO) and Kyoto Encyclopedia of Genes and Genomes (KEGG) using the "clusterProfiler" package with a threshold of $P<0.05$. The DEGs were then imported into the Metascape database for enrichment analysis at $P<0.01$. The results were visualized.

Random forest trees and gene importance analysis

The "randomForest" package was used to filter the DEGs and identify disease signature genes with gene importance scores greater than 2, and to draw random forest trees and gene importance maps.

Gene scoring and ANN model construction

The disease signature genes were scored using the R software package "Limma," and the upregulated genes with expression greater than their median values were scored as 1 and those less than their median values as 0. The downregulated genes with expression greater than their median values were scored as 0 and those less than their median values as 1. The ANN prediction models were constructed using the "neuralnet" and "NeuralNetTools" packages. The accuracy of the ANN model was then predicted using the "pROC" package, and the results were visualized.

Validation of diagnostic marker expression and diagnostic value

The value of gene prediction in the RIAs and UIAs groups was determined using the independent data set GSE54083 as a validation set. The diagnostic effect of disease versus control samples was determined

based on the area under the curve (AUC) of the ROC curve. The results were visualized using P<0.05 as the threshold.

Immune cell infiltration and immune cell differential analysis

CIBERSORT was analyzed for immune cell infiltration with a threshold of P< 0.05, and the samples with high reliability were selected to obtain the relative content of 22 immune cell infiltrates in each sample. Correlations between immune cells were analyzed using the "corrplot" software package. The "vioplot" software package was used to analyze and visualize the differences between the immune cells of the experimental and control samples.

Results

Expression of DEGs

GSE13353 and GSE36791 were combined as the analysis data set, which included 54 ruptured IA samples (experimental group) and 26 unruptured IA samples (control group). After differential analysis, 27 DEGs, including 26 upregulated genes and 1 downregulated gene, were screened and displayed by applying the heat map and the volcano map (Fig. 1)

Enrichment analysis of DEGs

GO and KEGG enrichment analyses of DEGs were performed to screen enrichment results with an actual probability of P<0.05 (Fig. 2A,2B). The GO results suggested that the biological processes associated with DEGs mainly included myeloid leukocyte activation, regulation of immune effector processes, positive regulation of DNA-binding transcription factor activity, and myeloid leukocyte-mediated immunity. The DNA-KEGG results showed that DEG-associated pathways included neutrophil extracellular trap formation, fructose and mannose metabolism, transcriptional dysregulation in cancer, fluid shear stress, arterial dysregulation, fluid shear stress and atherosclerosis, amebiasis, and leukocyte transendothelial cell migration. The enrichment analysis after importing DEGs into the Metascape database showed (P< 0.01) that the DEGs were related to interleukin (IL) signaling pathway, neutrophil degranulation, positive regulation of DNA-binding transcription factor activity, inflammatory response, and IL-18 signaling pathway (Fig. 2C).

Random forest trees and gene importance analysis

The number of trees corresponding to the point with the lowest error in the cross-validation of the experimental group, the control group, and all samples was 153, which was obtained by filtering the DEGs through a random forest tree plot (Fig. 3A). Further analysis of this point resulted in a gene importance score (Fig. 3B). Disease signature genes with scores greater than 2 were filtered out, including hexokinase 3 (HK3), matrix metalloproteinase 9 (MMP9), CST7, NCF2, and uridine phosphorylase 1 (UPP1). Subsequent heat map analysis of these five disease signature genes (Fig. 3C) showed that the samples from the experimental and control groups could be roughly closely clustered, indicating that the

expression of the disease signature genes could be distinguished from that in the experimental group. This further confirmed that the five genes were signature genes of RIAs.

ANN model analysis and diagnostic value

The ANN model (Fig. 4) could be divided into three layers: the input layer included the five characteristic genes of RIAs, the hidden layer was obtained according to the scoring of the disease characteristic genes, and the output layer was obtained according to the corresponding weights, the five nodes of the hidden layer, and their weights. The output layer was the sample attributes. The results suggested that the *MMP9* and *UPP1* genes reached the hidden layer and the output layer with greater weights, respectively, indicating that the two predicted the sample with greater accuracy. The next ROC curve results suggested that the ANN model predicted the sample attributes with an accuracy of AUC = 0.947 (95% CI 0.900–0.983) in the analysis data set (Fig. 5A) and AUC = 0.825 (95% CI 0.475–1.000) in the validation data set (Fig. 5B), which proved that this ANN model was used to predict sample attributes with high confidence.

Immune cell infiltration and immune cell differential analysis

A total of 22 immune cells were selected, including 12 types of intrinsic immune cells, activated dendritic cells, unactivated dendritic cells, activated mast cells, unactivated mast cells, activated natural killer (NK) cells, unactivated NK cells, macrophages (M0, M1, and M2), monocytes, neutrophils, and eosinophils, and 10 types of adaptive immune cells, including plasma cells, naive B cells, CD8+ T cells, naive CD4+ T cells, memory B cells, activated CD4+ memory T cells, unactivated CD4+ memory T cells, follicular helper T cells, regulatory T (Treg) cells, and γδ T cells. The samples from UIA and RIA groups were analyzed for immune cell infiltration and immune cell differences (Fig. 6). The numbers of CD8+ T cells ($P < 0.001$), activated CD4+ memory T cells ($P = 0.01$), unactivated CD4+ memory T cells ($P = 0.039$), Treg cells ($P < 0.001$), activated NK cells ($P = 0.002$), unactivated NK cells ($P = 0.007$), macrophages M0 ($P < 0.001$), and neutrophils ($P < 0.001$) showed statistically significant differences in expression compared with that in the UIA group. Among these, the numbers of CD8+ T cells, activated CD4+ memory T cells, unactivated CD4+ memory T cells, activated NK cells, macrophage M0, and neutrophils were higher in the RIA group. In contrast, the numbers of Treg cells and unactivated NK cells were high in the UIs group. Positive correlations were found on immune cell correlation analysis between the numbers of eosinophils and macrophages M1 ($r = 0.65$), eosinophils and activated dendritic cells ($r = 0.43$), and unactivated CD4+ memory T cells and CD8+ T cells ($r = 0.43$). Negative correlations were found between the numbers of neutrophils and CD8+ T cells ($r = -0.69$), Treg cells and activated CD4+ memory T cells ($r = -0.51$), and neutrophils and unactivated CD4+ memory T cells ($r = -0.47$).

Discussion

IA rupture is the most common cause of nontraumatic subarachnoid haemorrhage, with a high rate of death and disability. Current treatment for UIAs is primarily evaluated based on patient age, aneurysm size and location. However there is no high level of evidence to guide clinical efforts. Therefore understanding the genetic differences and immune cell infiltration between RIAs and UIAs and

constructing predictive models related to RIAs by these genes is essential for early prevention, diagnosis and treatment of IA.

In this study, 28 DEGs between RIAs and UIAs were screened, 27 of which were upregulated and 1 was downregulated. GO and KEGG enrichment analyses showed that the differential gene expression was mainly associated with inflammatory response, immune response, fluid shear stress, and atherosclerosis, which were key factors influencing the pathophysiological changes in RIAs. The results of Metascape enrichment analysis further confirmed this conclusion. Rachel Kleinloog et al. found that the lysosomal pathway played a key role in IA rupture and was closely associated with the immune response [6]. Cebral et al. studied nine aneurysms and found areas of abnormally high wall shear stress (WSS); the arterial wall showed thinning and sclerosis, which, in turn, led to rupture and bleeding. Therefore, it was assumed that abnormal hemodynamics led to a significant increase in WSS, which, in turn, allowed progressive degeneration of the arterial wall layer to form aneurysms [7]. Intracranial atherosclerosis was also a common cause of RIAs, which could lead to the destruction of the elastic layer of the artery and thinning of the arterial wall, thus inducing rupture and bleeding [8]. All of the aforementioned findings were consistent with our enrichment results and confirmed the accuracy of this study.

Five disease signature genes were derived using random forest tree and gene importance scoring algorithms: HK3, MMP9, CST7, NCF2, and UPP1. HK is an enzyme that catalyzes the transfer of phosphate from ATP to glucose in the first step of glucose metabolism and has four important isozymes [9]. HK3 is expressed at low levels in most tissues. However, Lin et al. found that HK3 was abundantly expressed in infiltrating leukocytes and also rapidly increased in activated macrophages and astrocytes in Sprague–Dawley rats with spinal cord injury, suggesting that the *HK3* gene was involved in processes such as injury, inflammation, apoptosis, and cell survival [10, 11]. CST7 encoded a cysteine peptidase inhibitor-cystatin F, which was stably expressed in NK and CD8 + T cells. Sawyer et al. found that CST7 was significantly upregulated in sepsis and a range of bacterial, viral, and sterile inflammatory conditions [11]. NCF2 encodes nicotinamide adenine dinucleotide phosphate oxidase in humans [12]. It can be induced by tumor necrosis factor-α (TNF-α) and interferon-γ [13]. TNF-α upregulates NCF2 expression, promotes reactive oxygen species production, and activates MMPs and the p38 MAPK pathway, which further enhances the inflammatory response [14]. *MMP9* is a member of the MMP family and is mainly involved in the reorganization and degradation of the extracellular matrix. Tronc et al. found that the inflammatory response in the aneurysmal vessel wall and the proteolytic effect of MMPs on the extracellular matrix of the vessel led to the destruction of the intra-arterial elastic lamina, which induced aneurysm rupture [15]. An investigation of a mouse model of IA showed that the application of broad-spectrum inhibitors of MMPs significantly reduced the formation of IAs in mice [16]. The enzyme encoding UPP1 catalyzes the reverse phosphorylation of uridine (or 2'-deoxyuridine) and plays a role in the degradation and metabolism of pyrimidine ribonucleosides. In a study of genetic data from patients with glioma, Wang et al. found that genes positively associated with UPP1 were mainly involved in immune and inflammatory responses, especially in the activation of T cells [17]. All of the aforementioned five disease-characterizing genes were expressed in various immune and inflammatory

responses, and further clarification of their mechanisms of action could be of significant help in predicting the risk of rupture hemorrhage in patients with IA and in early clinical intervention.

Subsequently, the infiltration analysis of immune cells showed that the numbers of CD8 + T cells, activated CD4 + memory T cells, unactivated CD4 + memory T cells, activated NK cells, macrophage M0, and neutrophils were high in the RIA group. In contrast, the numbers of Treg cells and unactivated NK cells were higher in the UIA group. In a study of 27 patients with IA, Zhang et al. found an imbalance of CD4 + T cells in the peripheral blood of patients, manifested by increased activity of T helper (Th)1 and Th17 cells and decreased activity of Th2 and Treg cells, which might enhance the cell-mediated inflammatory response and thus aggravate the disease [18]. Macrophages are key effector cells in the development of IA [19]. Kanematsu et al. found in a mouse IA model that the inflammatory cells that accumulated in the aneurysm wall were mainly macrophages. Compared with wild-type mice, MCP-1 knockout mice (mice with reduced monocyte/macrophage numbers and impaired macrophage function) had a significantly lower incidence of IA, confirming the critical role of macrophages in the development of IA [20]. Inflammatory cell infiltration produces a large number of inflammatory cytokines such as nuclear factor-κB (NF-κB) and TNF-α, which played a key role in the activation, regulation, and migration of immune cells. NF-κB (nuclear factor-κ-gene binding) is a key transcription factor in arterial endothelial cells and is closely associated with IA rupture [21]. A rat aneurysm model showed that a lack or inhibition of NF-κB significantly reduced the activation and production of downstream proinflammatory factors and could inhibit IA formation and progression [22, 23]. Ali et al. discovered through *in vitro* and *in vivo* experiments that TNF-α decreased the expression of contractile genes and increased the expression of proinflammatory and pro-matrix-remodeling genes in cerebrovascular smooth muscle cells (SMCs). This led to a shift from a contractile phenotype to an inflammatory/matrix-remodeling phenotype in SMCs, which eventually induced aneurysm rupture [24]. Fewer studies exist on the interconnections between immune cells associated with RIAs. The number of osinophils was found to be positively correlated with the numbers of macrophages M1, activated dendritic cells, unactivated CD4 + memory T cells, and CD8 + T cells. The numbers of neutrophils negatively correlated with the numbers of CD8 + T cells, unactivated CD4 + memory T cells, and Treg cells with activated CD4 + memory T cells. However, further experiments are needed to verify the mechanisms of immune cell interactions and their specific effects on the rupture of RIAs.

In conclusion, the formation and rupture of IAs is a complex process involving abnormal changes in blood flow, immune and inflammatory responses, and vascular wall remodeling. Recent studies suggest that IAs occur at the apex of the bifurcation or in the curved outer wall of the vessel with abnormal hemodynamics. Under the effect of high shear stress, the morphology and function of vascular endothelial cells are altered. NF-κB is hyperactivated, thus promoting the expression of inflammatory factors, including cyclooxygenase-2 and prostaglandin E2 [21]. It also induces the activation of monocyte chemotactic protein 1 and vascular cell adhesion molecule 1, which allows macrophage recruitment and adhesion. Macrophages then release other proinflammatory molecules, including TNF-α, IL-1β, metalloproteinases, and other proteases, and the integrity of the intravascular elastic lamina and extracellular matrix is further disrupted, gradually leading to the formation of aneurysms and rupture.

Conclusions

The association of disease-characterizing genes obtained from our analysis with RIAs has not yet been experimentally confirmed. Extensive clinical trials are required to validate and analyze their potential value as the predictive markers of IA rupture. Also, a large number of molecular experiments are needed to explore the infiltration of various types of immune cells and their inter-relationships so as to further clarify the mechanism of RIA development, which is important for our understanding of the disease.

Declarations

Acknowledgements

We sincerely acknowledge the GEO database for providing online resources for gene expression and the researchers for uploading their meaningful datasets. We also sincerely appreciate the contributions of all participants to our present study.

Authors' contributions

Q-FH conceived and designed the experimental procedure. QJ and W-HS performed the experiments and analyzed the data. QJ wrote the manuscript. Q-FH, QJ, W-HS and X-JL revised the manuscript. S-QS and J-JS organized the images. All authors read and approved the final manuscript.

Funding

The present study was supported by the Natural Science Foundation of jiangsu Province (BK20130386), the National Natural Science Foundation

of China (81402447), the Chinese Projects for Postdoctoral Science Funds (no. 2015M571792), the Jiangsu Planned Projects for Postdoctoral Research Funds (no. 1402200C).

Data availability

All raw data used in this study were obtained from the public GEO database(https://www.ncbi.nlm.nih.gov/geo/).

Ethics approval and consent to participate

Not applicable.

Consent for publication

Not applicable.

Competing interests

The authors declare that they have no competing interests.

Author details

[1]Department of Neurosurgery, Affiliated Hospital of Nantong University, No.20, Xisi Road, Nantong 226006, China.

[2]Department of Medicine, Nantong University, No.19, Qixiu Road, Nantong 226006, China.

[3]Department of Cardiovascular Medicine, The First Affiliated Hospital of Guangxi Medical University, No. 22, Shuangyong Road, Nanning 530021, China.

References

1. Muhammad S, Hänggi D. Inflammation and Anti-Inflammatory Targets after Aneurysmal Subarachnoid Hemorrhage. Int J Mol Sci. 2021 Jul 8;22(14):7355.
2. Du GJ, Geng D, Zhou K, et al. Identification of potential key pathways, genes and circulating markers in the development of intracranial aneurysm based on weighted gene co-expression network analysis. Artif Cells Nanomed Biotechnol. 2020 Dec;48(1):999-1007.
3. Nakaoka H, Tajima A, Yoneyama T, et al. Gene expression profiling reveals distinct molecular signatures associated with the rupture of intracranial aneurysm. Stroke. 2014 Aug;45(8):2239-45.
4. Tulamo R, Frösen J, Hernesniemi J, et al. Inflammatory changes in the aneurysm wall: a review. J Neurointerv Surg. 2018 Jul;10(Suppl 1):i58-i67.
5. Renganathan V. Overview of artifi cial neural network models in the biomedical domain. Bratisl Lek Listy. 2019;120(7):536-540.
6. Kleinloog R, Verweij BH, Vlies P, et al. RNA Sequencing Analysis of Intracranial Aneurysm Walls Reveals Involvement of Lysosomes and Immunoglobulins in Rupture. Stroke. 2016 May;47(5):1286-93.
7. Cebral JR, Vazquez M, Sforza DM, et al. Analysis of hemodynamics and wall mechanics at sites of cerebral aneurysm rupture. J Neurointerv Surg. 2015 Jul;7(7):530-6.
8. Kataoka K, Taneda M, Asai T, et al. Structural Fragility and Inflammatory Response of Ruptured Cerebral Aneurysms A Comparative Study Between Ruptured and Unruptured Cerebral Aneurysms. Stroke. 1999 Jul;30(7):1396-401.
9. Clemons TA, Toledo-Pereyra LH. Hexokinase: A Glycolytic Enzyme with an Inflammatory Ischemia and Reperfusion Connection. J Invest Surg. 2015;28(6):301-2.
10. Lin YH, Wu Y, Wang Y, et al. Spatio-temporal expression of Hexokinase-3 in the injured female rat spinal cords. Neurochem Int. 2018 Feb;113:23-33.
11. Sawyer AJ, Garand M, Chaussabel D, et al. Transcriptomic Profiling Identifies Neutrophil-Specific Upregulation of Cystatin F as a Marker of Acute Inflammation in Humans. Front Immunol. 2021 Apr 1;12:634119.

12. Denson LA, Jurickova I, Karns R, et al. Clinical and genomic correlates of neutrophil reactive oxygen species production in pediatric patients with crohn's disease. Gastroenterology. 2018 Jun;154(8):2097-2110.
13. Cunninghame Graham DS, Morris DL, Bhangale TR, et al. Association of NCF2, IKZF1, IRF8, IFIH1, and TYK2 with systemic lupus erythematosus. PLoS Genet. 2011 Oct;7(10):e1002341.
14. Huang LF, Li X, Chen ZP, Liu YJ. Identification of inflammation-associated circulating long Non-coding RNAs and genes in intracranial aneurysm rupture-induced subarachnoid hemorrhage.Mol Med Rep. 2020 Dec;22(6):4541-4550.
15. Tronc F, Mallat Z, Lehoux S, et al. Role of matrix metalloproteinases in blood flow-induced arterial enlargement: Interaction with NO. Arterioscler Thromb Vasc Biol.2000 Dec;20(12):E120-6.
16. Nuki Y, Tsou TL, Kurihara C, et al. Elastase-induced intracranial aneurysms in hypertensive mice. Hypertension.2009;54:1337-1344.
17. Wang J, Xu SH, Lv W, et al. Uridine phosphorylase 1 is a novel immune-related target and predicts worse survival in brain glioma. Cancer Med. 2020 Aug;9(16):5940-5947.
18. Zhang HF, Zhao MG, Liang GB, et al. Dysregulation of CD4(+) T Cell Subsets in Intracranial Aneurysm. DNA Cell Biol. 2016 Feb;35(2):96-103.
19. Shao L, Qin XP, Liu J, et al.Macrophage Polarization in Cerebral Aneurysm: Perspectives and Potential Targets. J Immunol Res. 2017;2017:8160589.
20. Kanematsu Y, Kanematsu M, Kurihara C, et al. Critical roles of macrophages in the formation of intracranial aneurysm. Stroke. 2011 Jan;42(1):173-8.
21. Pawlowska E, Szczepanska J, Wisniewski K, et al. NF-kB-Mediated Inflammation in the Pathogenesis of Intracranial Aneurysm and Subarachnoid Hemorrhage. Does Autophagy Play a Role? Int J Mol Sci. 2018 Apr 19;19(4):1245.
22. Aoki T, Kataoka H, Ishibashi R, et al. Reduced collagen biosynthesis is the hallmark of cerebral aneurysm: Contribution of interleukin-1βand nuclear factor-κB. Arterioscler Thromb Vasc Biol. 2009 Jul;29(7):1080-6.
23. Aoki T, Kataoka H, Shimamura M, et al. NF-kB is a key mediator of cerebral aneurysm formation. Circulation. 2007 Dec 11;116(24):2830-40.
24. Ali MS, Starke RM, Jabbour PM, et al. TNF-αinduces phenotypic modulation in cerebral vascular smooth muscle cells: implications for cerebral aneurysm pathology. J Cereb Blood Flow Metab. 2013 Oct;33(10):1564-73.

Figures

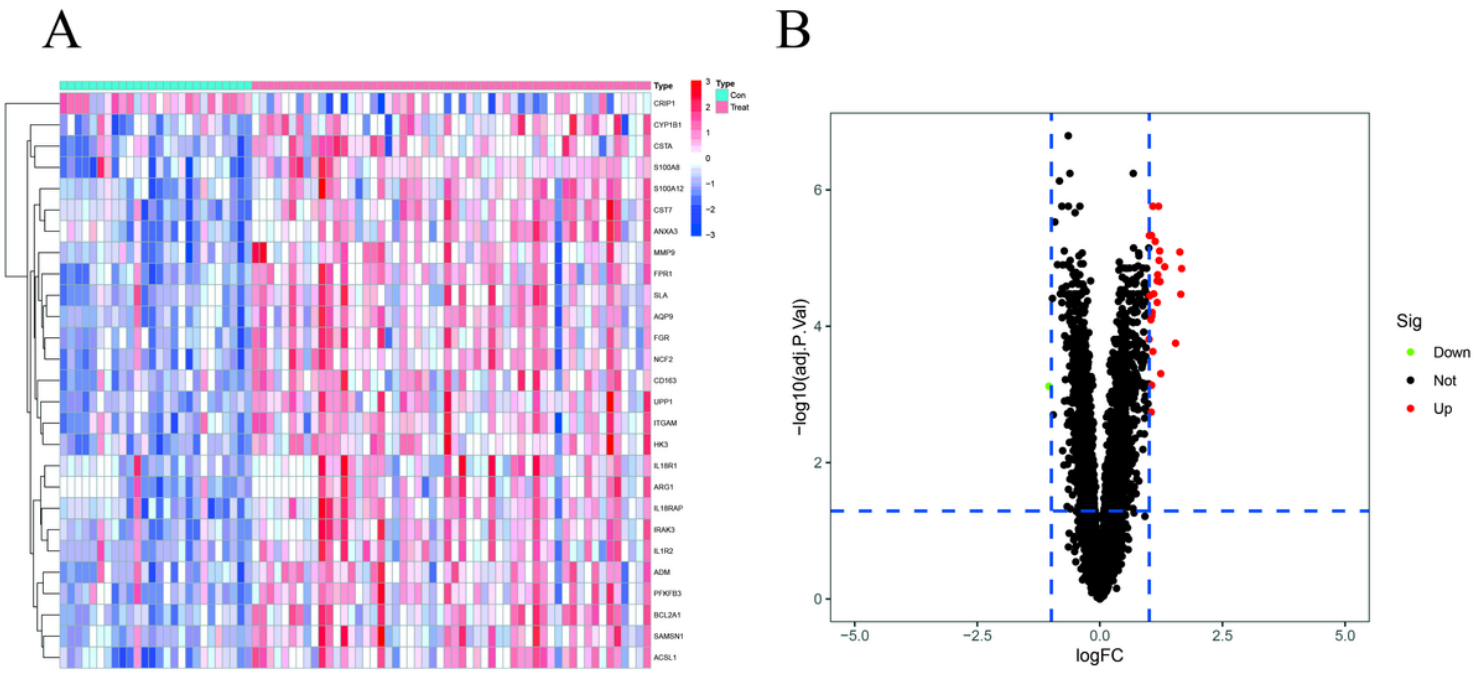

Figure 1

Heat map(A) and volcano map of differentially expressed genes(B).

(Note: In (A), red represents high expression and blue represents low expression. In (B), red represents upregulated genes and green represents downregulated genes.)

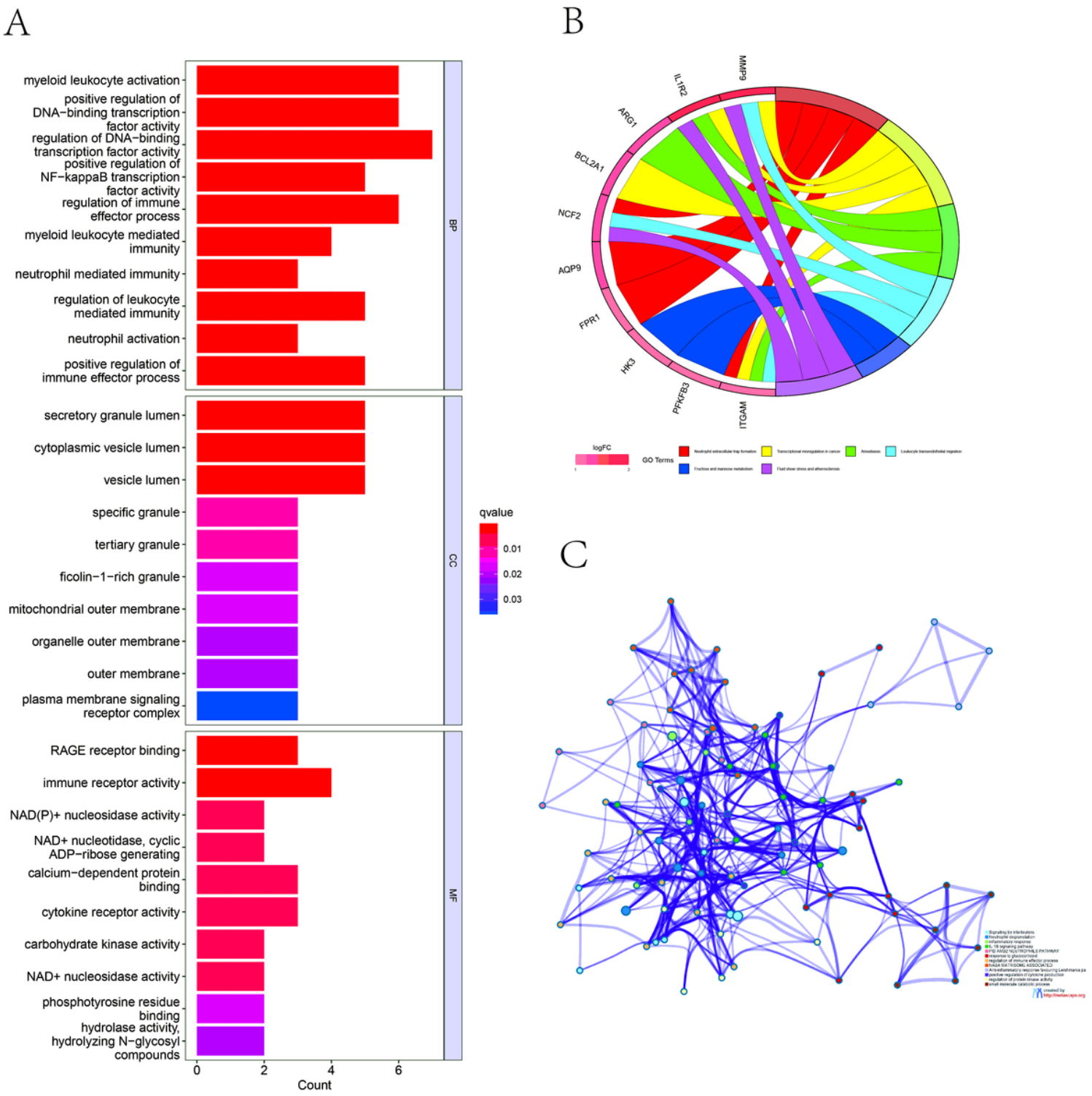

Figure 2

GO enrichment analysis (A), KEGG pathway enrichment analysis (B) and Metascape analysis(C).

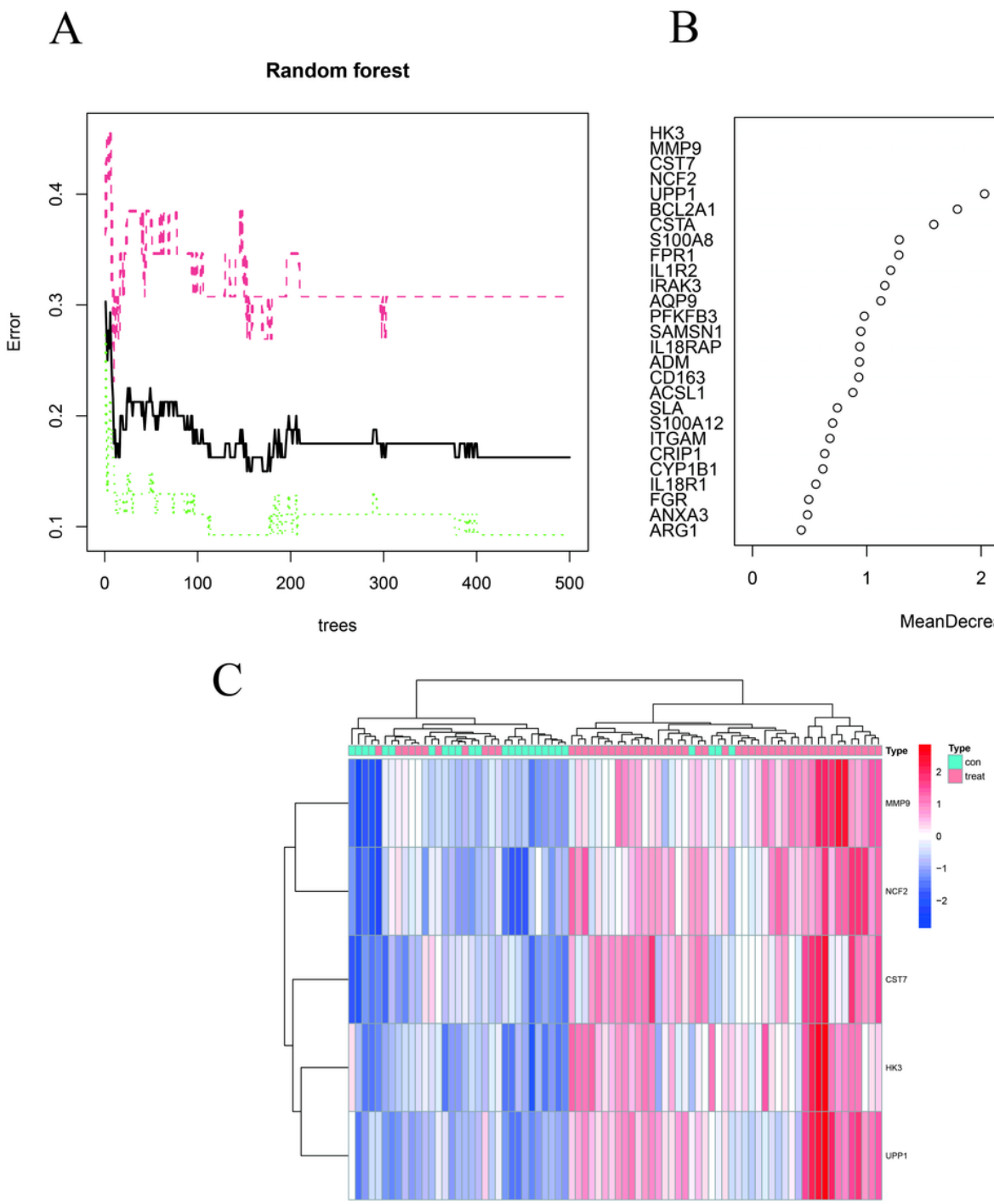

Figure 3

Random forest tree diagram(A), Gene importance map (B) and heat map of genes characterized by RIAs (C).

(Note: A:The horizontal axis indicates the number of trees. The vertical axis represents the error of cross-validation. Red indicates the error in the experimental group. Green indicates the error in the control group. Black indicates the error of all samples. B:Horizontal axis indicates the gene importance score and the vertical axis indicates the gene name. C:Horizontal axis indicates the control and experimental samples

and the vertical axis indicates the gene name. Red represents high expression. Blue represents low expression.)

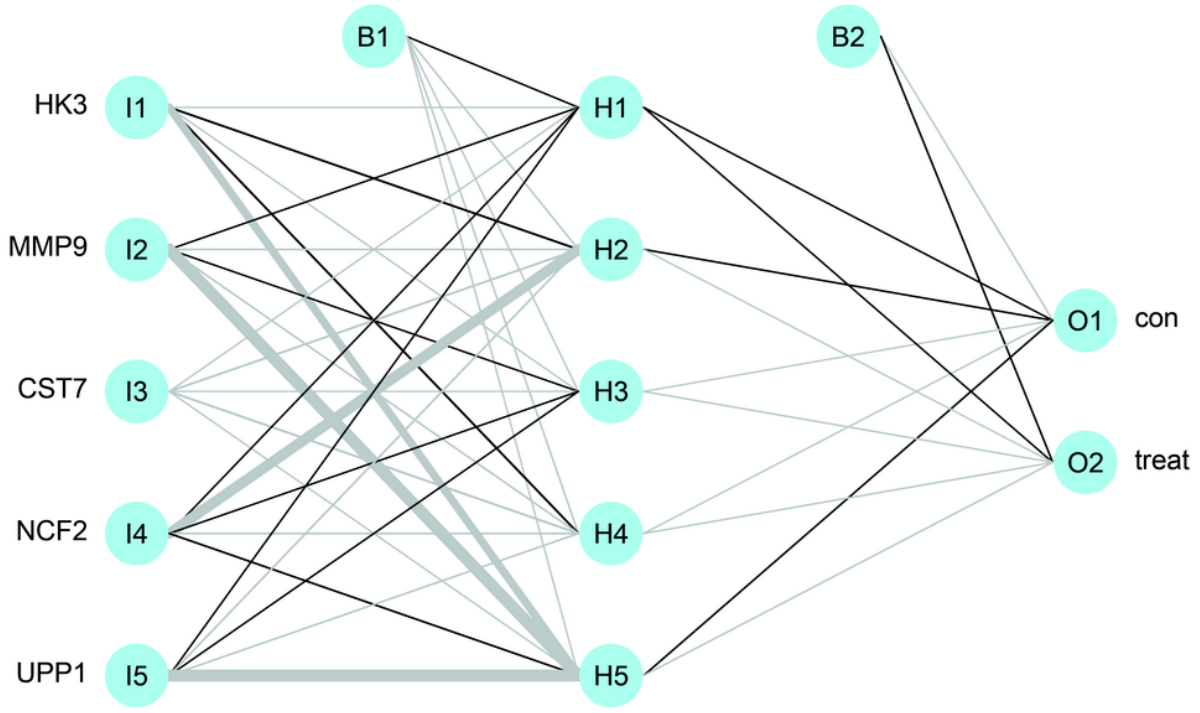

Figure 4

Artificial neural network model.

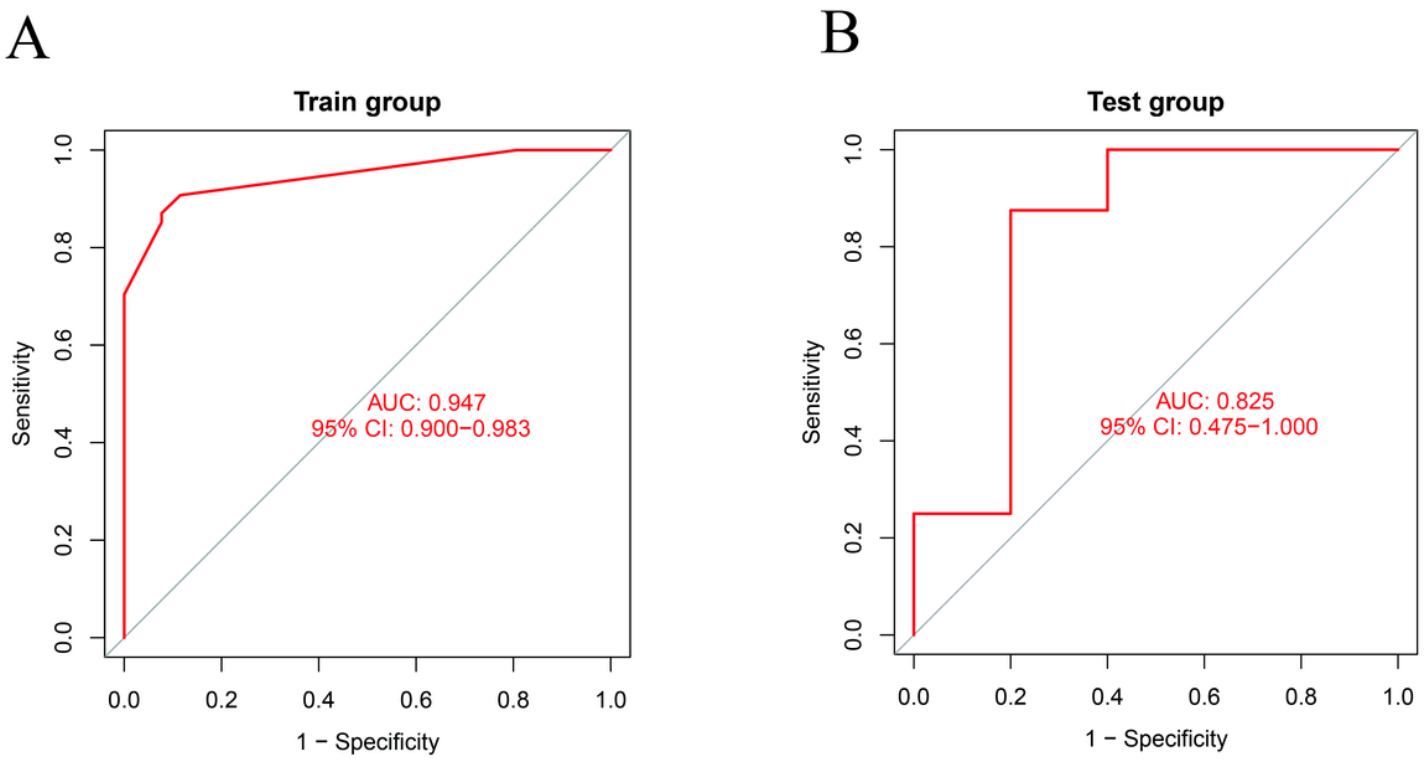

Figure 5

ROC curve.

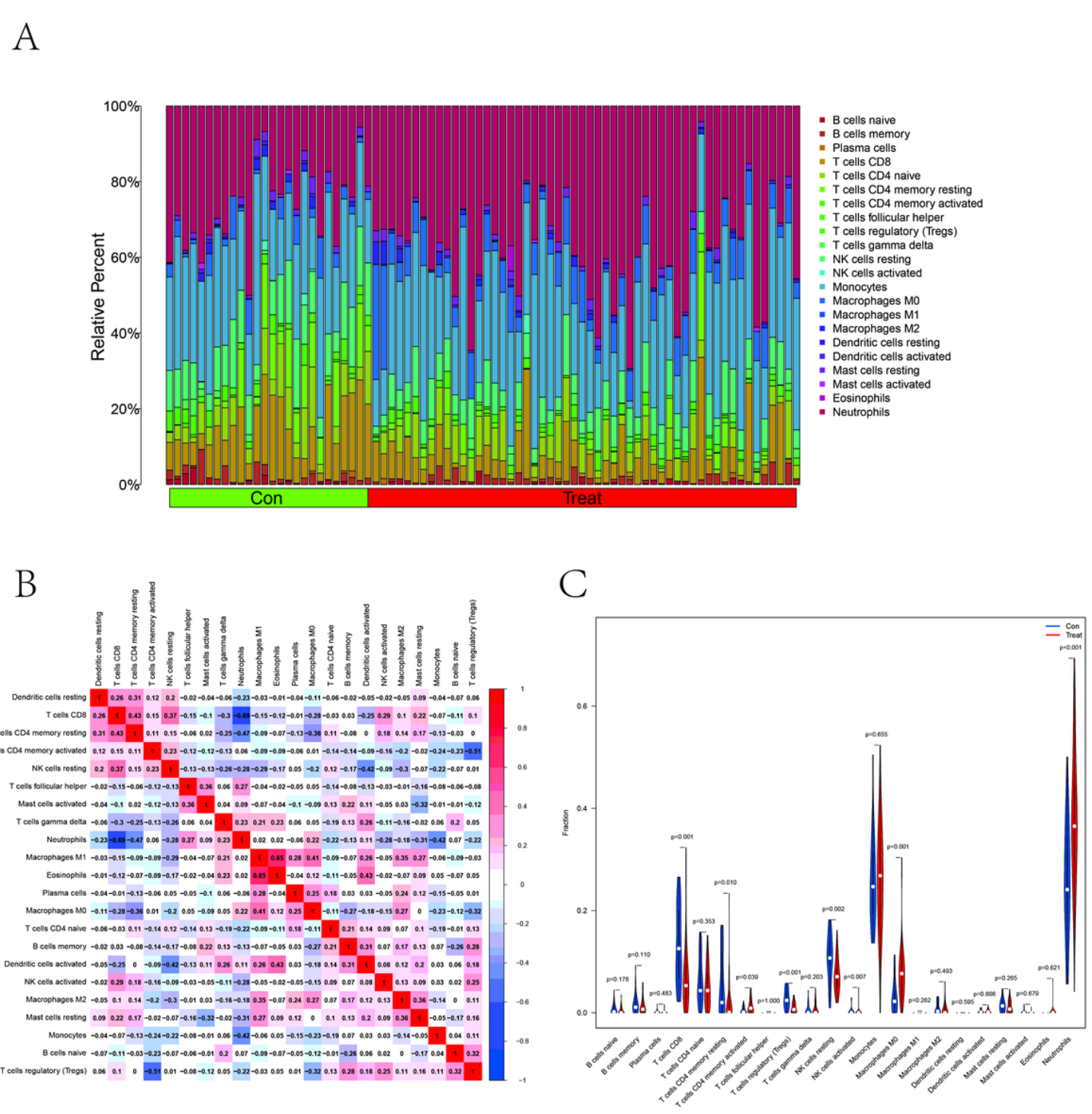

Figure 6

Distribution of 22 immune cells in UIAs and RIAs(A), correlation analysis between immune cells (B) and Violin plot of immune cell differential analysis(C).

(Note: A:The horizontal axis denotes the control and experimental group samples. The vertical axis denotes the percentage of various immune cell contents.C:The horizontal and vertical axes denote the names of immune cells. Red boxes indicate a positive correlation, blue ones indicate a negative correlation, and the values represent correlation coefficients.)